DOI: http://dx.doi.org/10.22104/ijhfc.2017.2342.1144

Iranian Journal of Hydrogen & Fuel Cell 1(2017) 37-52

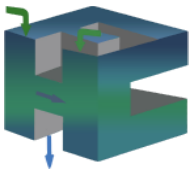

Iranian Journal of Hydrogen & Fuel Cell

IJHFC

Journal homepage://ijhfc.irost.ir

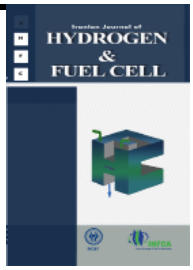

Three-dimensional modeling of transport phenomena in a planar anode-supported solid oxide fuel cell

Iman Mohammad Ebrahimi[1], Mohammad H. Eikani[2,*]

[1] **Department of Chemical and Polymer Engineering, South Tehran Branch, Islamic Azad University, Tehran, Iran**
[2] **Department of Chemical Technologies, Iranian Research Organization for Science and Technology (IROST), Tehran, Iran**

Article Information

Article History:

Received:
26 May 2017
Received in revised form:
04 Aug 2017
Accepted:
23 Aug 2017

Keywords

Solid oxide fuel cells
Anode-supported
Modeling
Radiation heat transfer
Optimization simulation

Abstract

In this article three dimensional modeling of a planar solid oxide fuel cell (SOFC) was investigated. The main objective was to attain the optimized cell operation. SOFC operation simulation involves a large number of parameters, complicated equations (mostly partial differential equations), and a sophisticated simulation technique; hence, a finite element method (FEM) multiphysics approach was employed. This can provide 3D localized information within the fuel cell. In this article, SOFC efficiency improvement has been investigated based on optimization parameters. For the first time, radiation heat transfer equations were considered in addition to the effects of conduction and convection heat transfer in 3D simulation in a planar cell. This effect has been neglected in all previous SOFCs simulations. Based on the proposed equations, the emissivity effect on temperature distribution was studied. The maximum location is where temperature and hydrogen mass fraction are high in the fuel. Radiation heat transfer between the channel wall and the fluid and also in between the cell and ambient outside have been employed. Minimizing the ohmic drop by optimizing the cathode layer thickness is another new aspect in this research. According to this optimization simulation, it is possible to achieve maximum current density.

1. Introduction

Solid oxide fuel cells, as very impressive sources of electrical energy, have attracted significant attention during the past decade [1]. A fuel cell is an energy transformation system which transforms chemical energy straightly into electrical energy without any harmful effect on the environment.

*Corresponding Author's Fax: +98-21-56276265
E-mail address: eikani@irost.ir

doi:10.22104/ijhfc.2017.2342.1144

Since the conversion from chemical to electrical energy is direct, less energy loss is incurred during transformation [2]. It is very important to study the effects of different parameters on the performance of a SOFC and for this purpose an experimental or numerical simulation method can be adopted as the research method. Numerical simulation involves constructing a mathematical model of the SOFC and using specifically designed software programs that allows the user to retouch the model to evaluate the system performance under various configurations and in real time [3, 4]. Numerical simulation can give accurate, consistent and efficient results. Modeling allows testing and development of new materials, fuels, geometries and operating conditions without disrupting the existing system configuration [5]. In addition, it is possible to measure internal variables which are experimentally difficult or impossible to measure and study the effects of various operating parameters on generated power, efficiency, current density, maximum temperatures reached, stresses caused by temperature gradients and effects of thermal development for electrolytes, electrodes and interconnects [6]. A Schematic diagram of mass and charge flows in a SOFC is shown in Fig. 1.

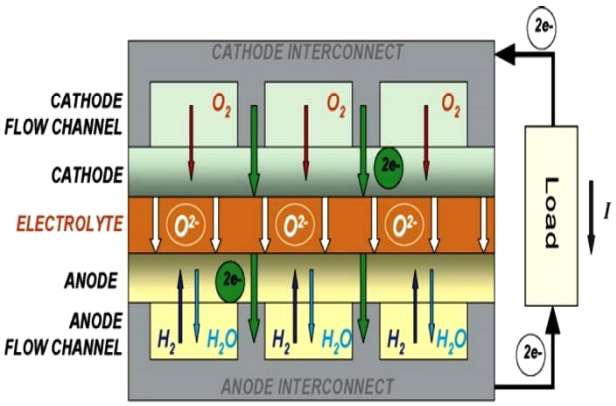

Fig. 1. Schematic diagram of mass and charge flows in a SOFC [43]

For more than two decades, a number of sophisticated mathematical models have been published for planar, tubular and monolithic designs [7, 8]. Mathematical models of SOFCs are important tools in understanding and examining effects of various design and operation parameters on SOFC performance, as well as helping in SOFC expansion [9]. Modeling results can be used to optimize designs and select optimal operation conditions [10]. Numerical modeling of SOFCs has been associated with some levels of uncertainty. These arise from some unknown physical properties, many model reductions, limitations of numerical computations, etc. Many published simulations use a simple polarization curve for validation [5-8].

The aim of the study presented in this paper is to investigate the transport phenomena inside a single SOFC fed with hydrogen as the fuel and to evaluate its overall performance. For this purpose a three-dimensional CFD model has been developed for an anode-supported planar SOFC [11]. With the modeling results, the distribution of temperature, flow velocity, the gas concentrations (fuel and air) through the cell structure and gas channels is discussed.

In addition to the heat conduction and convection caused by the SOFC's high operating temperature, the effect of radiation heat transfer has been evaluated [12].

It is important to know the optical properties of the relevant surfaces when determining surface-to-surface radiation. In all encountered articles the relevant surface is assumed to be 'grey', which means the properties are independent of wavelength [13-16].

Electric potential and current density distributions over the cell and fuel utilization are also computed. The electrochemical reactions, over-potentials and related electric parameters throughout the cell are calculated using COMSOL software [21].

2.Modeling

In a SOFC, electrical conduction, radiation and convection heat transfer, gas phase mass transport, chemical reactions and ionic conduction take place simultaneously and are tightly coupled. Conservation laws are applied to each domain

to obtain a comprehensive model containing all the above mentioned phenomena. This model is implemented in COMSOL Multiphysics (Ver. 5.2) software and all equations are solved at the same time [17, 18, 19].

2.1. Geometry and physics

A single cell of a planar cross-flow and anode supported SOFC is considered for modeling. The model incorporates the conservation of mass, energy and momentum and also charge balance, secondary current and Butler–Volmer equations. Some of the assumptions employed in the modeling are as follows:

i. Gas mixture is treated as an ideal gas;
ii. Flow is laminar due to the low Reynolds number;
iii. Isothermal conditions and
iv. Gas diffusion layer (GDL) are made of isotropic and homogeneous porous materials.

It should be said that isothermal conditions are a common assumption in single SOFCs [22].

Assumed emissivity values found in the literature for the cathode surface are listed in Table 1 [13-20].

Table 1. Cathode and anode surface emissivity [13- 20]

Emissivity ε_{cath}	Reference	Emissivity ε_{an}	Reference
1	[13]	1	[19]
0.9	[14]	0.9	[20]
0.8	[15]	0.55	[15]
0.7	[16]		
0.55	[17]		
0.35	[18]		

Figs. 2 and 3 show the computational domain of the model. The domain includes a section of the ceramic membrane, both electrodes, and gas flow channels under equal configurations. The values of the geometrical and physical model parameters are listed in Table 2.

The superiority of the this work over other modeling procedures is related to its optimizing reaction and cathode layers' thickness which produce regular and better pass of electrical current to achieve a lower ohmic loss and maximum current density [22].

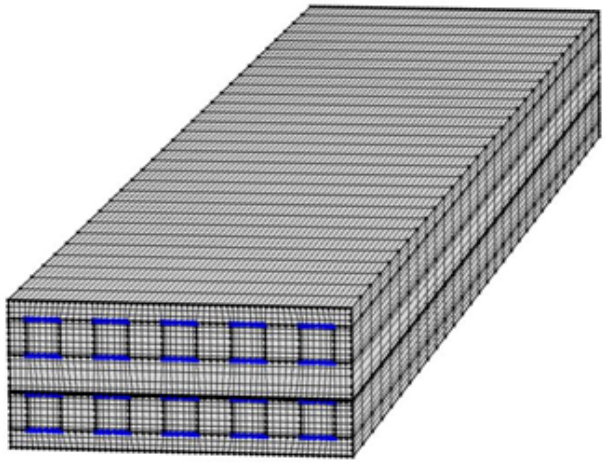

Fig. 2. Computational domain of the model.

Table 2.The SOFC dimensions[23, 24]

Element		Value
L	Cell length	5 cm
H_ch	Channel height	1 mm
W_ch	Channel width	1 mm
W_rib	Rib width	1 mm
H_inter	Interconnect height	0.5 mm
W_inter	Interconnect width	2 mm
H_ASL	Anode supportlayer height	1 mm
H_ARL	Anode reaction layer height	20 mm
H_E	Electrode height	8 mm
H_CRL	Cathode reaction layer height	20 mm
H_CDL	Cathode diffusion layer height	13 mm

The parameters H, W and L represent the width, height and length of the cell, respectively. The indices C, A and E represent channels, cathode reaction layer (CRL), cathode diffusion layer (CDL), anode reaction layer (ARL), anode spread layer (ASL) and the electrolyte. In Table 3, φ_i and ε_i represent the pore volume fraction and porosity. Also, τ_i shows the ratio of twist and curvature of the pass between two points and $\in_i$ shows the permeability porous. These four parameters affect fluid velocity and concentration in porous areas. Other parameters in Table 3 are σ_i and d_{i-j} which represent the electrical conductivity of layers and distribution coefficient of component i^{th} in the j^{th} component, respectively. M_i and ρ_i represent the molar

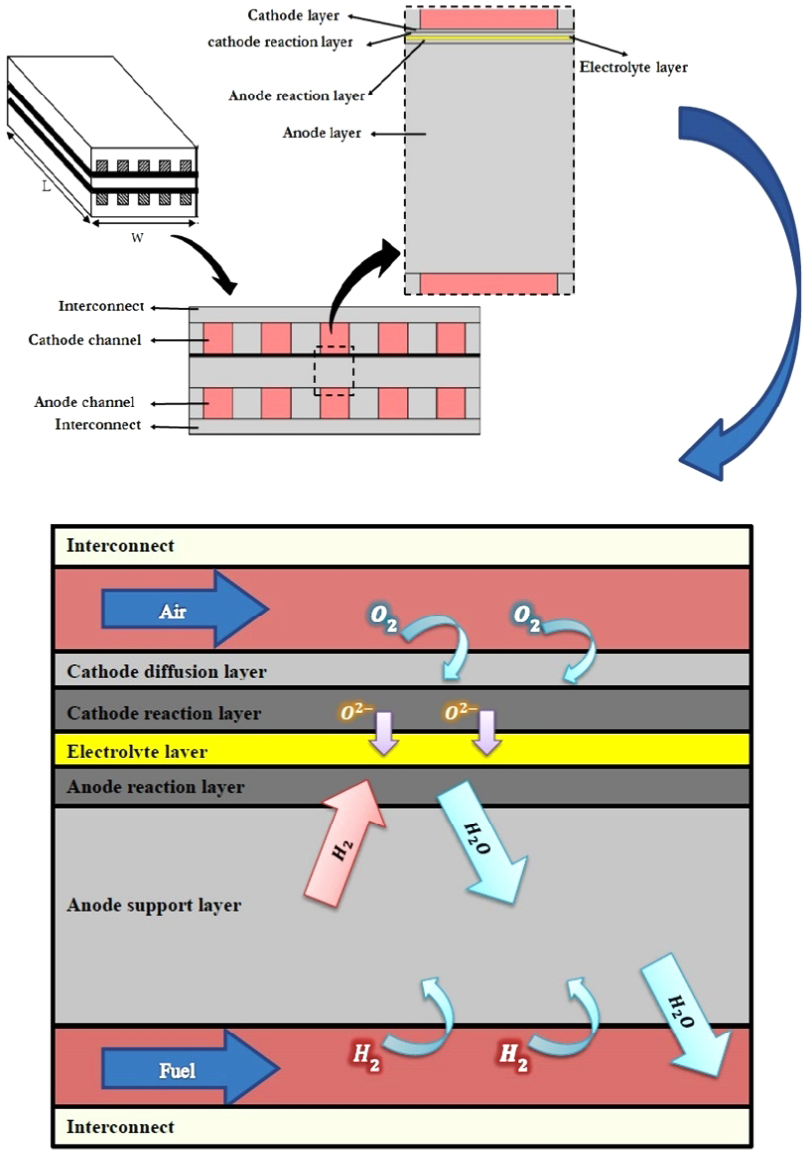

Fig. 3. Detailed anode-supported SOFC components

mass and density of fluid. Cell voltage was selected as the variable parameter in this simulation. For each cell current density, a certain value for the cell voltage is obtained. Using those data, it will be possible to draw voltage vs. current density.

Table 4 represents the input parameters of the model including temperature reference, concentration, fluid inlet velocity, inlet mole fraction and mass fraction of the components.

2.2. Governing equations

Governing equations bring together all the relevant parameters and variables involved in the SOFC process and define their relationship to each other. In a SOFC different types of processes are happening at the same time. The governing equations can be classified into three types of models as follows:

• Flow model, or fluid dynamics model: accounts for all the fluid flow physics.

• Thermal or heat transfer model: accounts for the energy transfer involved through exchange of heat between components.

• Electrochemical model: accounts for all the electrochemical processes happening between different species in a SOFC [22].

Table 3. The SOFC physical properties [24, 25]

Parameter	Value e	Scope changes
φ_CRL	0.587	0.2-0.8
φ_CDL	1	0.2-0.8
φ_ARL	0.4	0.2-0.8
φ_ASL	0.4	0.2-0.8
ε_CRL	0.4	0.2-0.8
ε_CDL	0.36	0.2-0.8
ε_ARL	0.097	0.2-0.8
ε_ASL	0.42	0.2-0.8
τ_i	3	1-10
∈_CRL	5.4×10^{-14} m^2	-
∈_CDL	3.7×10^{-14} m^2	-
∈_ARL	3.4×10^{-14} m^2	-
∈_ASL	3.4×10^{-14} m^2	-
∈_CRL	1.011×10^{5} s/s	-
σ_CDL	1.011×10^{5} s/s	-
σ_ARL	9.3×10^{3} s/s	-
σ_ASL	1.52×10^{4} s/s	-
σ_inter	1.13×10^{6} s/s	-
d_H_2_H_2O	8.6147×10^{-4} m^2/s	-
d_O_2_H_2O	2.4589×10^{-4} m^2/s	-
d_N_2_H_2O	2.4556×10^{-4} m^2/s	-
d_O_2_N_2	1.9297×10^{-4} m^2/s	-
M_{H2}	0.002 kg/mol	-
M_{N2}	0.028kg/mol	-
$M_{H2\,O}$	0.018kg/mol	-
M_{O2}	0.032 kg/mol	-
ρ_anode	0.02797kg/m^3	-
ρ_cathode	0.3246kg/m^3	-
p_ref	1atm	0.98-1
V_cell	1.05 V	0.4-1.05

The most important mathematical equations describing the whole process in a SOFC are as follows [23]:

2.2.1. Continuity equation

$$\rho\nabla.u = 0 \qquad (1)$$

In this equation ρ is the fluid density and u is the velocity field.

2.2.2. Navier-Stokes equation

Navier-Stokes equations for incompressible fluids are generally used for a fuel cell due to the small velocities [24]. These equations describe the flow regime through open domains like the flow channels.

Table 4.Input parameters

Parameter	Value	Scope changes
T	800 °C	700-1000
C_{O2_ref}	2.38 mol/m^3	-
C_{H2_ref}	10.78 mol/m^3	-
U_a	5.0363 m/s	1-6
U_c	13.149 m/s	3-15
X_{H2}	0.97	0-1
$X_{H2\,O}$	0.03	0-0.3
X_{O2}	0.21	0.21-1
X_{N2}	0.79	0-0.79
$w_{H2\text{-}in}$	0.78226	0-1
$w_{H2\ o\text{-}in}$	0.21774	-
$w_{o2\text{-}in}$	0.23301	-
$w_{N2\text{-}in}$	0.76699	0-0.77

$$\rho(u.\nabla)u = \nabla.\left[\mu\left(\nabla u + (\nabla u)^T\right)\right] - \nabla P \qquad (2)$$

2.2.3. Brinkman equation

Brinkman equations for incompressible flow through porous media, like the electrodes, were applied. The Brinkman equations are composed of the continuity and momentum equations for porous media, given by:

$$\frac{\mu}{\kappa}u = \nabla.\left[\frac{1}{\varepsilon}(\mu\left(\nabla u + (\nabla u)^T\right)\right] - \nabla P \qquad (3)$$

k is the fluid permeability in the porous medium and ∇P represents the fluid pressure gradient [24].

Maxwell-Stefan equation

The multispecies mass transport in the computational domain, which comprises the gas channels and GDL, is described by the Maxwell–Stefan equation. The flux of each species is solved in terms of mass fraction. The general form of the Maxwell–Stefan equation is shown below [25-26].

$$\left[-\rho w_i \sum D_{ij}^{eff}\left(\nabla x_j + \left(x_j - w_j\right)\frac{\nabla P}{P}\right) + \rho w_i u\right] = S_i \qquad (4)$$

The effective diffusion coefficient (D_{ij}^{eff}) is calculated

by the Knudsen formula as follows:

$$D_{ij}^{eff} = \frac{\varepsilon}{\tau}\left(\frac{1}{D_{ij}} \times \frac{1}{D_{iK}}\right)^{-1} \quad (5)$$

$$D_{ij} = 3.16\times10^{-8}\frac{T^{1.75}}{P\left(v_i^{1/3}+v_j^{1/3}\right)^2}\left(\frac{1}{M_i}-\frac{1}{M_j}\right)^{1/2} \quad (6)$$

$$D_{iK} = \frac{97}{2} d_{pore}\sqrt{\frac{T}{M_i}} \quad (7)$$

$$d_{pore} = \frac{2}{3}\frac{\varepsilon}{1-\varepsilon} d_p \quad (8)$$

The electrochemical reaction is modeled by placing mass sources and sinks for the reactants and products, respectively, in correspondence with the computed rates in the anode and cathode regions neighboring the electrolyte. And source (S) terms for each component in the Maxwell-Stefan equation (Eq. 4) are defined as follows [27]:

$$S_{O_2} = \frac{-J_c M_{O_2}}{4F}, S_{H_2} = \frac{-J_a M_{H_2}}{2F}, S_{H_2O} = \frac{J_a M_{H_2O}}{2F} \quad (11, 10, 9)$$

Eqs. (9) and (10) yield the stoichiometric amounts of the oxygen and hydrogen. In practice, the amounts of hydrogen and oxygen fed to the fuel cell are in excess of their stoichiometric values as shown in Eqs. (12) and (13).

$$S_{H_2}^{in} = n_a \frac{j_a}{2F} M_{H_2} \quad (12)$$

$$S_{O_2}^{in} = n_c \frac{j_c}{2F} M_{O_2} \quad (13)$$

2.2.4. Ohm's Law equations

It is used to express the principle of conservation of charge and ion Ohm's law equations which are defined as follows [28]:

$$-\sigma_{el}\nabla^2\varphi_{el} = S_{el} \quad (14)$$

$$-\sigma_{io}\nabla^2\varphi_{io} = S_{io} \quad (15)$$

Source term S_{el} and S_{io} represent the generation and consumption rates of species resulting from the electrochemical reaction in the SOFC.

The anode reaction layer (ARL) is:

$$S_{io} = -S_{el} = j_a \quad (16)$$

And the cathode reaction layer (CRP) is:

$$S_{io} = -S_{el} = j_c \quad (17)$$

In the electrolyte layer we have:

$$S_{io} = 0 \quad (18)$$

2.2.5. Butler - Volmer equations

To express electrochemical kinetics of the reactions at the anode and cathode, the Butler-Volmer equation is used as follows [29, 30, 34]:

$$j_a = A_{Va} j_{0,ref}^{H_2}\left(\frac{C_{H_2}}{C_{H_2,ref}}\right)^{\gamma_{H_2}} \times \left\{\exp\left(\eta_a \frac{n\alpha_a F}{RT}\right) - \exp\left(-\eta_a \frac{n(1-\alpha_a)F}{RT}\right)\right\} \quad (19)$$

$$j_c = -A_{Vc} j_{0,ref}^{O_2}\left(\frac{C_{O2}}{C_{O_2,ref}}\right)^{\gamma_{O_2}} \times \left\{\exp\left(\eta_c \frac{n\alpha_c F}{RT}\right) - \exp\left(-\eta_c \frac{n(1-\alpha_c)F}{RT}\right)\right\} \quad (20)$$

α is the charge transfer coefficient and n is the number of electrons involved in the electrochemical reaction per mole reactant. For the electrochemical reaction at the anode and cathode layers (A_V) is calculated using the following equation:

$$A_V = \pi sin^2\theta r_{el}^2 n_t n_{el} n_{io} \frac{Z_{el} Z_{io}}{Z} p_{el} p_{io} \quad (21)$$

$$n_t = \frac{1-\varepsilon}{\left(\frac{4}{3}\right)\pi r_{el}^3\left[n_{el} + (1-n_{el})\left(\frac{r_{io}}{r_{el}}\right)^3\right]} \quad (22)$$

where θ is the contact angle between electron and ion conducting particles that is equal to 15°, r_{el} is the radius of the electron conducting particles that is equal to 1.0 μm. n_t is the total number of particles per unit volume, n_{el} and n_{io} are the number fraction of electron and ion conducting particles, and Z_{el}

and Z_{io} are the coordination number of electron and ion conducting particles. Z is the total average particle coordination number in the electrode which is equal to 6 and p_{el} and p_{io} are the probabilities for an electron and an ion conducting particle to belong to connecting ends of the composite [31-33]. All previous mentioned parameters are required to calculate A_V and are related to each other as shown here,

$$n_{el} = \frac{\varphi}{\left[\varphi + (1-\varphi)\left(\frac{r_{io}}{r_{el}}\right)^3\right]} \quad (23)$$

$$n_{io} = 1 - n_{el} \quad (24)$$

where φ is a volume fraction of the electron conducing particle in an electrode, which is equal to 0.5,

$$Z_{el} = 3 + \frac{Z-3}{\left[n_{el} + (1-n_{el})\left(\frac{r_{io}}{r_{el}}\right)^2\right]} \quad (25)$$

$$Z_{io} = 3 + \frac{(Z-3)\left(\frac{r_{io}}{r_{el}}\right)^2}{\left[n_{el} + (1-n_{el})\left(\frac{r_{io}}{r_{el}}\right)^2\right]} \quad (26)$$

$$P_{el} = \left[1 - \left(2 - \frac{Z_{el-el}}{2}\right)^{2.5}\right]^{0.4} \quad (27)$$

$$P_{io} = \left[1 - \left(2 - \frac{Z_{io-io}}{2}\right)^{2.5}\right]^{0.4} \quad (28)$$

$Z_{el\text{-}el}$ represents the average coordination number between electronic particles and $Z_{io\text{-}io}$ represents the average coordination number between ionic particles,

$$Z_{el-el} = \frac{n_{el} Z_{el}^2}{Z} \quad (29)$$

$$Z_{io-io} = \frac{n_{io} Z_{io}^2}{Z} \quad (30)$$

η in Eqs. (19) and (20) represents the anode and cathode activation loss, the loss occurs due to the energy required to start a chemical reaction which is defined as follows [35]:

$$\eta_a = \varphi_{el,a} - \varphi_{io,a} - E_{a,eq} \quad (31)$$

$$\eta_c = \varphi_{el,c} - \varphi_{io,c} - E_{c,eq} \quad (32)$$

In the above equations φ_{io} and φ_{el} are ion and electric potential, respectively. $E_{a,eq}$ and $E_{c,eq}$ are the equilibrium potential of the anode and cathode in reversible mode. Potential general equilibrium ($\Delta E_{eq}=E_{c,eq}-E_{a,eq}$) is obtained in the following manner, which is called the Nernst equation [36]:

$$\Delta E_{eq} = E_r - \frac{RT}{nF} \ln\left[\prod_i \left(\frac{p_i}{p_0}\right)^{\upsilon_i}\right] \quad (33)$$

If the fuel cell acts reversibly, the Gibbs free energy will be converted into electrical energy and provides the electrical energy necessary for the movement of electrons in the outer shell [37].

$$\begin{cases} Anode:\ H_2 + O^{2-} \rightarrow 2e^- + H_2O \\ Cathode:\ \frac{1}{2}O_2 + 2e^- \rightarrow O^{2-} \end{cases}$$

$$\Rightarrow \quad H_2 + \frac{1}{2}O_2 \rightarrow H_2O$$

For the above reaction :(ΔG=-237.3 kJ⁄mol at 25°C)

$$G = -nFE_r^0 \rightarrow E_r^0 = -\frac{\Delta G}{nF} \rightarrow E_r^0 = \frac{-237.3}{2 \times 96485} = 1.229\ V \quad (34)$$

E_r^0, voltage is reversible in standard mode.

$$\Delta E_r = E_r - E_r^0 = \frac{\Delta S}{nF}(T - 298.15)$$
$$\Rightarrow E_r = E_r^0 + \frac{\Delta S}{nF}(T - 298.15) \quad (35)$$

As a result:

$$\Delta E_{eq} = E_r^0 + \frac{\Delta S}{nF}(T - 298.15) - \frac{RT}{nF} \ln\left(\frac{p_{H_2O}}{P_{O_2}^{1/2}.P_{H_2}}\right) \quad (36)$$

The difference between real voltage and reversible voltage is based on irreversibility. Due to the irreversibility (voltage drops irreversible) during the processes, the real work in the fuel cell is less than the maximum useful work. The actual fuel cell

voltage is calculated as follows:

$$E_{cell} = \Delta E_{eq} - \Delta E_{eq,irrev} = \Delta E_{eq} - \left(\Delta E_{ohmic} + \Delta E_{act}\right) \quad (37)$$

ΔE_{act}, is the general activation loss, and ΔE_{ohmic}, is the ohmic loss, which is defined by Ohm's Law:

$$\Delta E_{ohmic} = IR_{ohmic} = iA_{cell}\left(\frac{\delta_{thick}}{\sigma A_{cell}}\right) = i\frac{\delta_{thick}}{\sigma} \quad (38)$$

In this equation, i is the current density of the unit ampere per square meter.

2.2.6. Energy equations (conduction, convection and radiation)

The electrochemical oxidation consists of two half-cell reactions occurring separately in the anode and cathode, and heat is generated within the electrolyte and the electrodes. The heat generated, however, is assumed to be produced within the anode structure because the cathode and electrolyte are very thin, relative to the anode [38].

The energy equation for the model is as follows. This equation is applicable to all areas, assuming that the displacement term is only intended for channels in porous media and it is ignored.

$$\nabla.\left(-\lambda\nabla T\right) = S_q - \rho C_p u.\nabla T \quad (39)$$

For porous media the equivalent thermal conductivity used are as follows:

$$\lambda = \left(1-\varepsilon\right)\lambda_{Porous} + \varepsilon\lambda_{fluid} \quad (40)$$

Source term in Eq. (39), for each segment is calculated as follows.

For the flow collector layer:

$$S_q = \sigma_{el}\nabla\varphi_{el}.\nabla\varphi_{el} \quad (41)$$

For the electrolyte layer:

$$S_q = \sigma_{io}\nabla\varphi_{io}.\nabla\varphi_{io} \quad (42)$$

For the anode reaction layer:

$$S_q = \sigma_{el}\nabla\varphi_{el}.\nabla\varphi_{el} + \sigma_{io}\nabla\varphi_{io}.\nabla\varphi_{io} + \frac{J_a}{nF}T\Delta S + J_a\eta_a \quad (43)$$

And for the cathode reaction layer:

$$S_q = \sigma_{el}\nabla\varphi_{el}.\nabla\varphi_{el} + \sigma_{io}\nabla\varphi_{io}.\nabla\varphi_{io} + \frac{J_c}{nF}T\Delta S + J_a\eta_c \quad (44)$$

The energy equation for the anode and cathode channel walls includes the pure radiation fluid (q_r) as follows:

$$n.\left(-\lambda\nabla T\right) = h\left(T_w - T_f\right) + q_r \quad (45)$$

Heat transfer coefficient in channels (h) using Nu is equal to 3.09 [40], which is calculated based on the following equation:

$$h = \frac{Nu\lambda_{gas}}{D_h} \quad (46)$$

Hydraulic diameter for the channel is also defined as:

$$D_h = \frac{2W_{CH}H_{CH}}{W_{CH} + H_{CH}} \quad (47)$$

As an innovation, radiation heat transfer equations were considered in a three dimensional state for a planar cell in the heat transfer section for the first time. In Equation 45, q_r, is the pure irradiation flux equal to the difference between radiation output flux from a surface and the input flux to it which is calculated based on the radiosity method as follows:

$$J = \rho G + \varepsilon E_b \quad (48)$$

In Eq. (48), G is the total irradiation in all directions and at all wavelengths per unit area, and J is the total irradiation output flux in all directions and at all wavelengths of radiation per unit area, which is equal to the sum of the intrinsic object (εE_b) and reflects part of the radiation emitted down to it (ρG). Given that $\alpha + \rho + \tau = 1$, assuming opaque surfaces, the transmission coefficient (τ) is zero. As a result, the total absorption coefficient and reflection coefficient are equal to one:

$$\alpha+\rho=1 \quad (49)$$

According to Kirchhoff's law, the absorption coefficient is equal to the diffusion coefficient:

$$\alpha=\varepsilon \quad (50)$$

And energy flux emitted from the black body (E_b) is calculated as follows:

$$E_b = \sigma T^4 \quad (51)$$

Where σ is the Stefan-Boltzmann constant 5.67×10^{-8} W/(m^2 K^4), and T is the temperature. According to Eqs. (48) to (51), the result will be:

$$J = (1-\varepsilon)G + \varepsilon\sigma T^4 \quad (52)$$

In the above equation, the light intensity level (G) is defined as follows:

$$G = G_m + F_{amb}\sigma T_{amb}^4 \quad (53)$$

In Eq. (54), the first sentence reflects the two-way radiation intensity between two surfaces and the second term shows radiation intensity of the environment to the channel wall.

$$G_m = \int_{S'}^{s} \frac{(-n'.r)(n.r)}{\pi|r|^4} J'dS \quad (54)$$

The energy equation for surfaces around the input and output spans is calculated by the following equation as well. The left term represents heat conduction transfer and the right term represents radiation from the fuel cell to the external environment.

$$n.(\lambda\nabla T) = \varepsilon\sigma(T_{amb}^4 - T^4) \quad (55)$$

2.3. Numerics

The model is computed using COMSOL Multiphysics software employing fully coupled solvers which solve the governing equations simultaneously using the Newton–Raphson iterations. The model is simulated with meshes of different sizes to check the grid independence. The final mesh size is described in Table 5. The convergence criteria was selected as10^{-6}. The Finite element method (FEM) of modeling is used to solve the partial differential equations (PDE) to express physical and scientific phenomena mathematically [41-42].

Table 5. Element sizes in the computational domain

Domain	Element size (mm)
Channels	0.1×10^{-3}
Electrodes	0.151×10^{-4}
Electrolyte	0.05×10^{-3}

For the research work presented here the 'Batteries and Fuel Cells' module has been used. The Batteries and Fuel Cells module enables the user to build models of electrodes and electrolytes in detail.

3.Results and discussion

Polarization is a state in which electrode surface potential shifts from its equilibrium value which leads to an electrochemical reaction. The polarization curve records voltage changes with current density, these data are very important in evaluating the performance of the fuel cell [36]. A fuel cell with good performance should show a curve with high current density in high voltage which expresses higher output power. In Fig. 4, the polarization curve obtained from the simulation and the point curve of the experimental results have been plotted. As shown, the model sufficiently matches experimental results.

The power curve can be used to show the rate of obtainable energy from this cell. Power is obtained from the polarization curve simply by multiplication of voltage by current, Fig. 5. The produced power in this cell is 11900W/m^2 in certain operating condition.

In Fig. 6, a three dimensional view of temperature distribution has been represented. At 0.75 volt as a medium voltage, the highest value of cell temperature is 1115 K and the lowest level was 1073 K. As can be seen, first the operating temperature is high because of a high concentration of hydrogen. As the electrochemical reaction consumes hydrogen decreasing output concentration and producing water the output temperature is reduced.

In Figs. 7-9 the effect of variation of cell temperature on voltage, power and ohmic drop has been plotted.

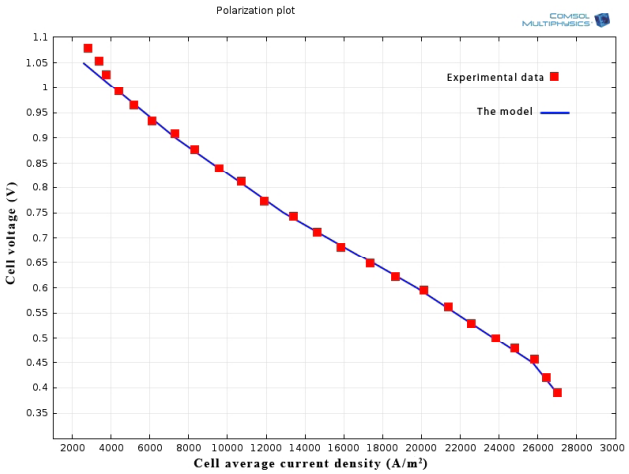

Fig. 4. Polarization Curve; Comparison between the model and experimental data [41].

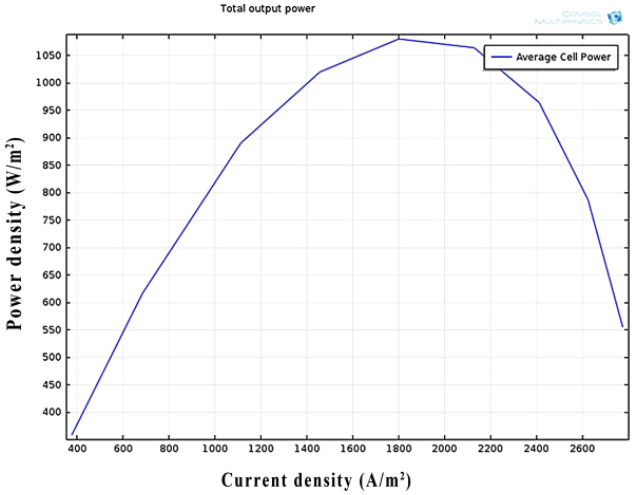

Fig. 5. Power density curve at average voltage.

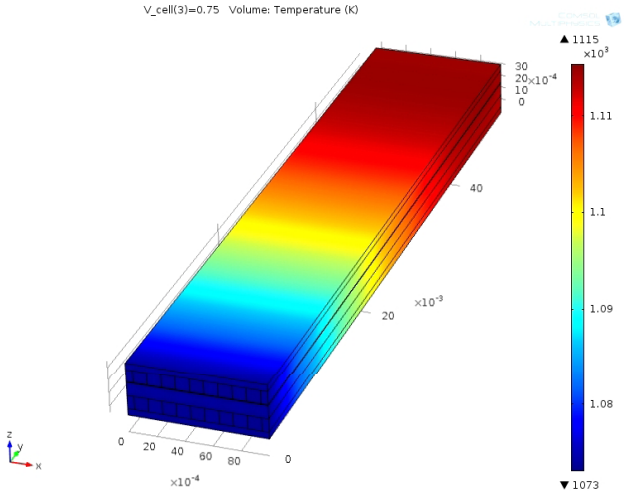

Fig. 6. 3D Temperature distribution

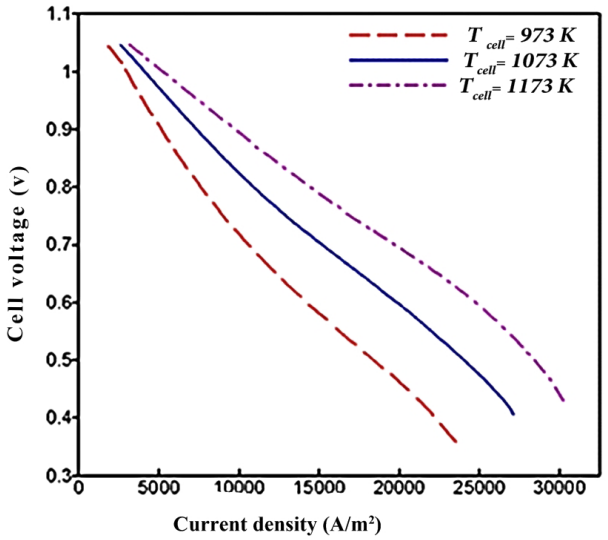

Fig. 7. Cell voltage vs. current density at three different temperatures.

Fig. 7 shows the variation of cell voltage with current density (current/area) for the cell operating at high and low temperatures. The initial fall in voltage is small for the cells operating at high temperatures, whereas the initial voltage fall is high for the cells operating at low temperatures. In addition to this, the cells operating at higher temperatures exhibit more linear behavior. As it can be observed in Fig. 7, the chart of cell voltage is plotted according to current density in three operating temperatures. It also shows that increasing the temperature under constant voltage significantly increases current density.

Fig. 8 represents power density vs. current density. It is clear from Fig. 8 that higher current density and power density usually occurs for low cell voltage. Hence to get maximum efficiency, the operating conditions should be balanced to get a good compromise between current density, voltage and operating cost. In the initial stages, activation polarization decreases the cell voltage. When current densities increase, the concentration losses are predominant and a sharp decrease in cell performance is observed. In a constant current density the increase in temperature increases power density of the cell significantly; so increasing temperature has a positive effect on cell power.

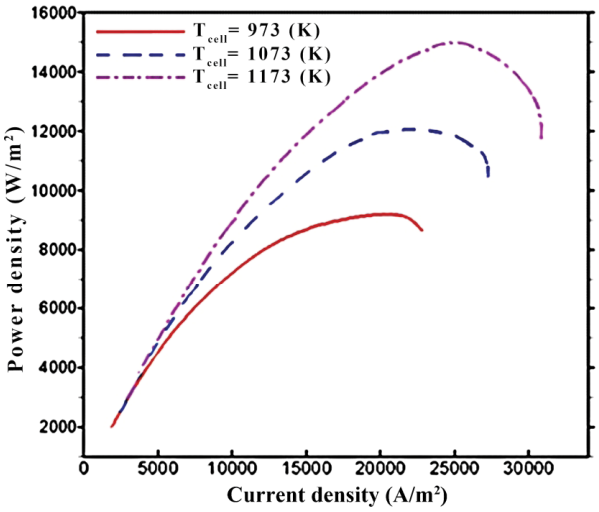

Fig. 8. Power density vs. current density at three different temperatures.

From Fig. 9, it can be concluded that ohmic drop decreases in a constant current density as temperature increases and this is a benefit for working a fuel cell and a better situation in cell efficiency.

Figs. 10, 11 and 12 show hydrogen in the anode side and oxygen and water molar concentrations in the cathode side, respectively. Fig. 10 has been plotted in 0.39 volt. It shows a concentration drop of hydrogen in the channel length and reaction layer (in the Y direction). Because of the electrochemical reactions, consumed hydrogen and produced water from oxidation of hydrogen are transferred to the channel and led out through the fuel channel.

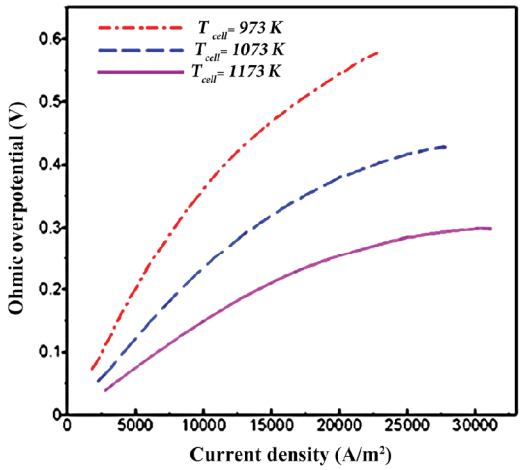

Fig. 9. Ohmic overpotential vs. current density at three different temperatures.

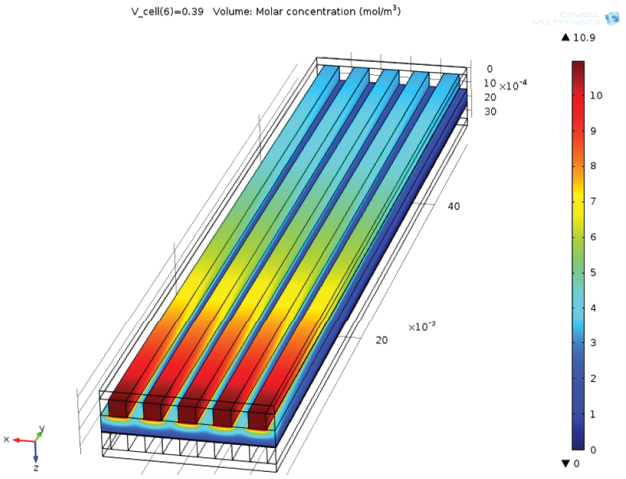

Fig. 10. Hydrogen concentration distribution in the anode.

In Fig. 11, the oxygen molar concentration has been displayed in the cathode at 0.39 volt. At the beginning, the amount of oxygen input (dark red) is high and after the reaction along the cell the rate of oxygen decreases 30 percent and is consumed along the cell. By considering the color, the rate ofoxygen decrease can be seen in the output of the channel (dark blue).

Fig. 12 is also plotted at 0.39 volt. The location of cathode input is y=L and the amount of input water is equal to the initial amount of water (0.34 mol/m^3); with the electrochemical reaction its amount increases until it reaches 1.55 mol/m^3. The main produced water is in the anode and exits through the output.

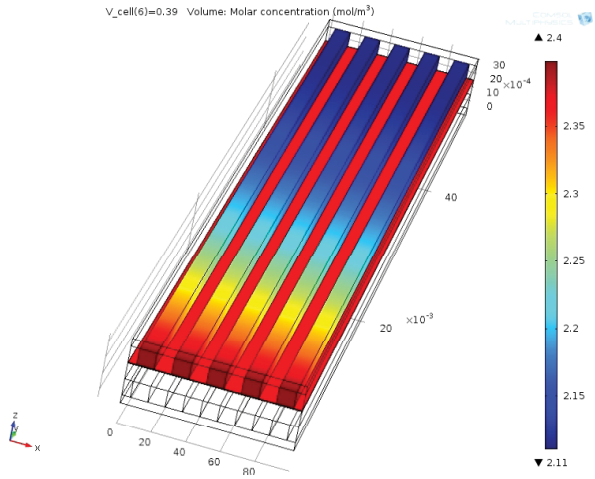

Fig. 11. Oxygen concentration distribution in the cathode.

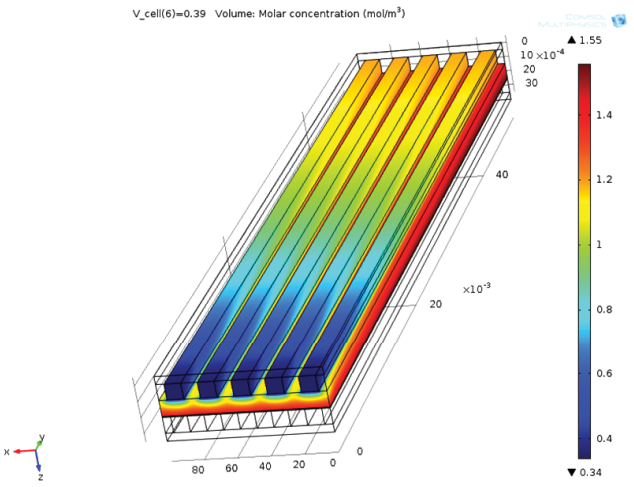

Fig. 12. Water concentration in the cathode.

Electric current and volumetric density distribution vectors in a section of cell for a channel have been represented in Fig. 13. As it can be seen, because of electrochemical potential difference created on both sides of the electrolyte, current from the anode collector (top level) flows to the negative pole (cathode) in order to be conducted to the anode side by an external circuit.

Minimizing the ohmic drop by optimizing the cathode layer thickness is another innovation in this article. Using this optimization, maximum current density is achieved. A noticeable point about this figure is that the widthwise electric current path in the cell occurs because of the low thickness of the cathode and the density of current in the middle part of the cell. This phenomenon increases the path length of the electric current flow and increases the ohmic loss. We can reduce this effect by considering an optimum thickness for the cathode and a more uniform current density distribution on the electrolyte surface.

The interesting point about the electric current path in the cell is a transverse electric current in the cathode that flows because of its low thickness and the density of current in the central region. This increases the flow path in the cathode as well as the ohmic drop . This effect can be reduced by considering the optimum thickness for the cathode and also by creating a uniform distribution of current density on the electrolyte surface.

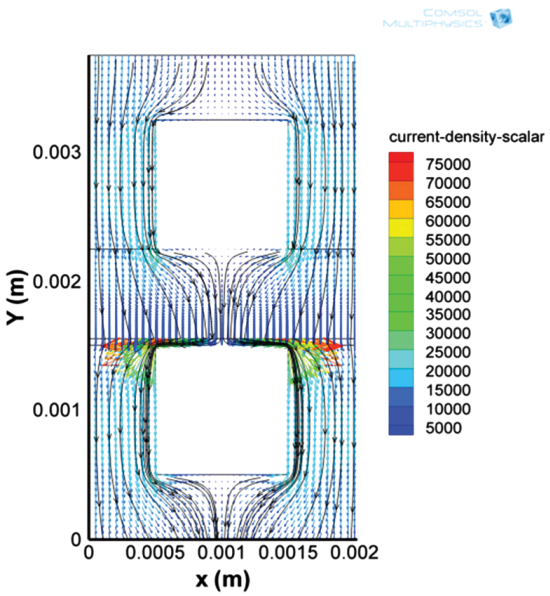

Fig. 13. Electrical current density vector and volumetric flow distribution on the electrode surface.

Fig. 14 shows the current density chart vs. emissivity coefficient at both co-current and countercurrent patterns. If the flow in the channels is co-current, temperature distribution will be more uniform than the state in which flow is countercurrent and temperature and current density will be more than when the flow is co-current.

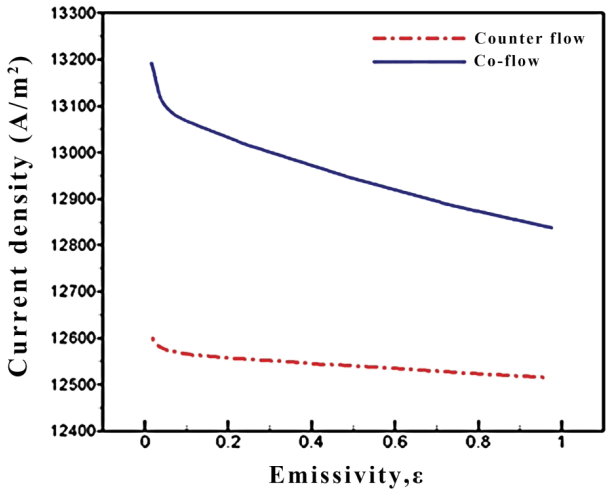

Fig. 14. Current density vs. emissivity coefficient at two different flow patterns.

Fig. 15 represents the current density chart according to the emissivity coefficient in two different voltages. When the emissivity coefficient increases, current

density decreases. As it can be observed in the temperature chart according to distance in different emissivity coefficients in Fig. 16, as the emissivity coefficient increases at a certain distance from the cell, the cell's operating temperature decreases and this reduces the current density and efficiency of the cell. Based on the results, considering the radiation effect in fuel cell, temperature and current density are reduced [26].

Figs. 17 and 18 present the cell voltage chart vs. current density and power density vs. current density with two different fuels, respectively. The use of a combination of hydrogen and carbon monoxide instead of hydrogen as fuel helps to improve the efficiency of the cell. Maximum power with hydrogen and carbon monoxide combined fuel is 214000 W/m^2. Fig. 19 displays the cell voltage vs. current density with two different type of oxidizers. Reactants such as oxygen or air electrochemically react at high temperature and generate electrical energy. This relationship relies on the fact that the electrolyte in SOFCs, such as YSZ, are pure ionic conductors and therefore only oxygen ions can permeate through the electrolyte to participate in the oxidation reaction at the anode/electrolyte interface. Using oxygen instead of air as the oxidation factor increases the current density. therefore only oxygen ions can permeate through the electrolyte to participate in the oxidation reaction at the anode/electrolyte interface. Using oxygen instead of air as the oxidation factor increases the current density.

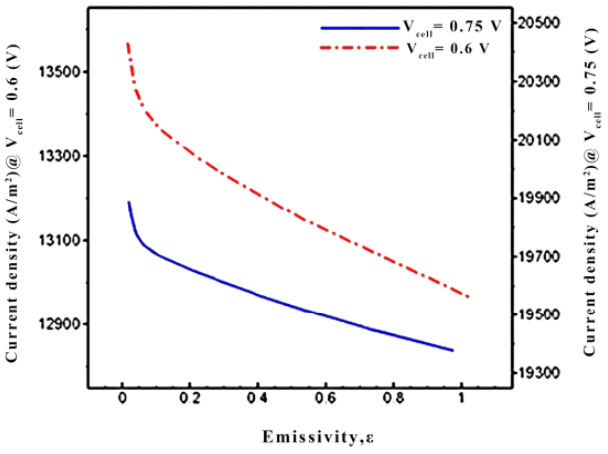

Fig. 15. Current density vs. emissivity coefficient in two different voltage.

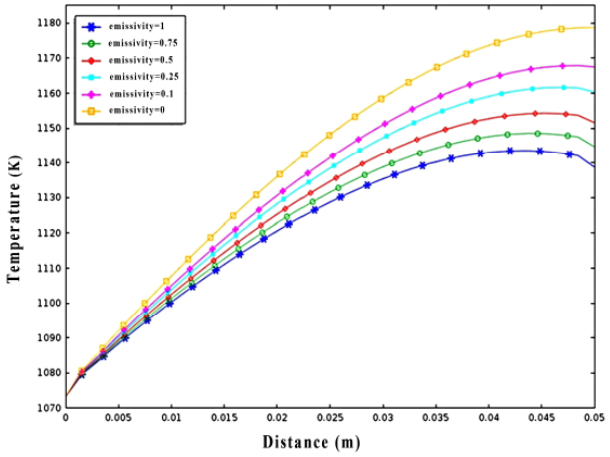

Fig. 16. Temperature vs. distance for different emissivity coefficients.

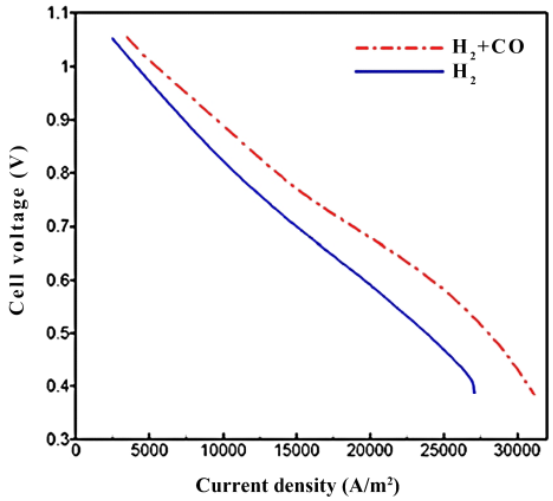

Fig. 17. Effect of fuel type on cell voltage.

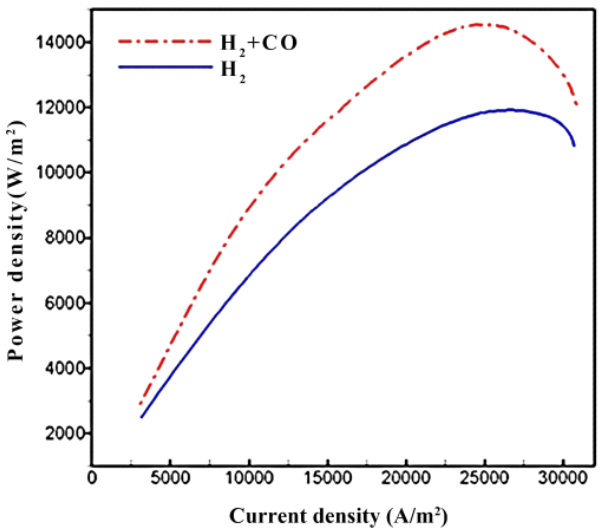

Fig. 18. Effect of fuel type on power density.

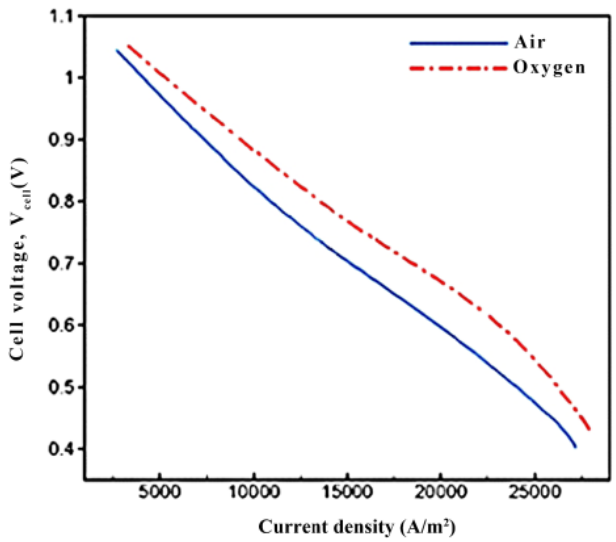

Fig. 19. Effect of oxidant type on cell voltage.

4. Conclusions

In this study, a three-dimensional modeling of transport phenomena has been developed and applied for an anode-supported planar SOFC. The simulation results of the developed model are in agreement with the experimental data obtained under the same conditions. Using the simulation results the distribution of temperature, fuel gas and oxygen concentrations through the cell components are presented and discussed. Potential and current density distributions in the cell and overall fuel utilization are also presented.

By optimizing the cathode thickness, vertical maximum current flow is observed. That uniform flow is moving with maximum current density. And only 5% of the current has been separated from the main track. Compared to similar papers this amount of reduction for current loss is very satisfying.

Operating temperature is one of the most important and the most effective factors in a solid oxide fuel cell plate because it has a significant effect on activation and ohmic drop. Each parameter that affects the fuel cell temperature can be an effective factor in solid oxide fuel cell efficiency. Based on the results, considering the radiation effect on the fuel cell, temperature and electric current density decrease. Also, by increasing the emissivity coefficient fuel cell l efficiency decreases because of increasing radiation flux to the environment, temperature and current density. Using oxygen instead of air as the oxidation factor increases the current density. The combined use of hydrogen and carbon monoxide instead of hydrogen as fuel helps to improve cell efficiency.

References

[1] Myung, J. H., Ko., H. J., Lee J. J., Hyun S. H., "Optimization of Distributed Cylindrical Interconnect Ribs for Anode- and Cathode-Supported Solid Oxide Fuel Cell", International Journal of Electrochemical Science, 2011, 6: 1617.

[2] Momirlan M., Veziroglu T., "Recent directions in world hydrogen production", Renew Sustain Rev, 1999, 3: 219.

[3] Ryan O'Hayre, Suk-Won Cha, Whitney Colella, Fritz B., Prinz., 3nd edition, Fuel Cell Fundamentals, Wiley, 2016.

[4] Subhash C. S., Kendall K.,1st ed., High-temperature Solid Oxide Fuel Cells, Fundamentals, Design and Applications, 2003.

[5] Yakabe H., Ogiwara T., Hishinuma M., Yasuda I., "3-D model calculation for planar SOFC", J Power Sources, 2001, 102: 144.

[6] Autissier N., Larrain D., Van Herle J., Favrat D, "CFD simulation tool for solid oxide fuel cells", J Power Sources, 2004, 131: 313.

[7] Andreassi L., Toro C., Ubertini S., "Modeling carbon monoxide direct oxidation in solid oxide fuel cells". In Proceedings ASME European Fuel Cell Technology and Applications Conference, 2007: 39057.

[8] Ni M, "2D thermal fluid modeling and parametric analysis of a planar solid oxide fuel cell", Energy Convers Manage, 2010, 51: 714.

[9] Pfafferodt M., Heidebrecht P., Stelter M., Sunmacher K., "Model-based prediction of suitable operating range of a SOFC for an Auxiliary power unit", J Power Sources, 2005, 149: 53.

[10] Andersson M., Yuan J., Sunde´n. B, "SOFC modeling considering electrochemical reactions at the active three phase boundaries", Int J Heat Mass Transfer, 2012, 55: 773.

[10] Andersson K. M. J., "Solid oxide fuel cell modeling at the cell scale", PhD thesis. Lund University, 2011.

[11] Goodenough, J.B., HuangY.H., "Alternative anode materials for solid oxide fuel cells", J. Power Sources, 2007, 173:1.

[12] Singhal S. C., "Solid Oxide Fuel Cells: Facts and Figures, Green Energy and Technology", Springer London, 2013: 23.

[13] Janardhanan V. M., Deutschmann O., "Numerical study of mass and heat transport in solid-oxide fuel cells running on humidified methane", Chemical Engineering Science, 2007, 62:18.

[14] Daun K.J., S.B. Beale., Liu F., Smallwood G.J., "Radiation heat transfer in planar SOFC electrolytes", Journal of Power Sources, 2006, 157: 302.

[15] Stiller C., Thorud B., Seljebo S., Mathisen O., Karoliussen H., Bolland O., "Finite-volume modeling and hybrid-cycle performance of planar and tubular solid oxide fuel cells", Journal of Power Sources, 2005, 141: 227.

[16] Calise F., Denticed'Accadia M., Restuccia G., "Simulation of a tubular solid oxide fuel cell through finite volume analysis: Effects of the radiative heat transfer and exergy analysis", International Journal of Hydrogen Energy, 2007, 32(17):4575.

[17] Gianfranco DiGiuseppe., "Surface-to-Surface Radiation Exchange Effects in a 3D SOFC Stack Unit Cell", Journal Of Fuel Cell Science And Technology, 2012, 9(6):1550.

[18] Suwanwarangkul R., Croiset E., Pritzker M.D., Fowler M.W., Douglas P.L., Entchev E., "Mechanistic modelling of a cathode-supported tubular solid oxide fuel cell", Journal of Power Sources, 2006, 154(1):74.

[19] Chaisantikulwat A., Diaz-Goano C., Meadows E.S., "Dynamic modelling and control of planar anode-supported solid oxide fuel cell", Journal of University of Alberta, 2006: 2365.

[20] Costamagna P., Costa P., Antonucci V., "Micro - Modeling of Solid Oxide Fuel Cell Electrodes", ElectrochimicaActa, 1998, 43: 375.

[21] COMSOL Multiphysics tutorial guide. "Current density distribution in Solid Oxide Fuel Cell"; 2012.

[22] Ni M., Leung DYC., Leung MKH., "Electrochemical modeling and parametric study of methane fed solid oxide fuel cells", Energy Convers Manage , 2009, 50(2):268.

[23] Raj A., Agus P. Sasmito,. T Shamim., "Numerical investigation of the effect of operating parameters on a planar solid oxide fuel cell", Energy Conversion and Management, 2015, 90:138.

[24] Kakaça S., Pramuanjaroenkij A., Zhoub X.Y., "A review of numerical modeling of solid oxide fuel cells", International Journal of Hydrogen Energy, 2007, 32: 761.

[25] Qua Z, Aravinda P.V., Dekker N.J.J., Janssen A.H.H., Woudstra N., Verkooijen A.H.M., "Three dimensional thermo-fluid and electrochemical modeling of anode-supported planar solid oxide fuel cell", Journal of Power Sources, 2010, 195: 7787.

[26] Dong S. K., Jung W. N, Rashid K., Kashimoto A., "Design and numerical analysis of a planar anode-supported SOFCstack", Renewable Energy, 2016, 637: 650.

[27] Campanari S., Iora P., "Definition and sensitivity analysis of a finite volume SOFC model for a tubular cell geometry", Journal of Power Sources, 2004, 132: 113.

[28] Todd B., Young J. B., "Thermodynamic and transport properties of gases for use in solid oxide fuel cell modelling", Journal of Power Sources, 2002, 110:186.

[29] Lee TS., Chung J., Chen Y-C., "Design and optimization of a combined fuel reforming and solid oxide fuel cell system with anode off-gas recycling", Energy Convers Manage, 2011,52: 3214.

[30] Meng Ni, Michael K.H. Leung., Dennis Y.C., Leung.,"A modeling study on concentration overpotentials of a reversible solid oxide fuel cell", Journal of Power Sources, 2006, 163: 460.

[31] Hosseini S., Ahmed K., Moses O. T., "CFD model of a methane fuelled single cell SOFC stack for analyzing the combined effects of macro/micro structural parameters", Journal of Power Sources, 2013, 234: 180.

[32] Ni M., Leung M., Leung D., "Parametric study of solid fuel cell performance", Energy Convers Manage, 2007, 48:1525.

[33] Sunden B., Faghri M., Transport Phenomena in Fuel Cells, WITPRESS, 2005.

[34] Su S., Gao X., Zhang Q., Kong W., Chen D.,"Anode-Versus Cathode-Supported Solid Oxide Fuel Cell: Effect of Cell Design on the Stack Performance", Journal of the Electrochemical science, 2015, 10: 2487.

[35] Huangfu Y, Gao F., Abbas-Turki A., Bouquain D, Miraoui A., "Transient dynamic and modeling parameter sensitivity analysis of 1D solid oxide fuel cell model", Energy Conversion and Management, 2013,71:172.

[36] Abhishek R., Tariq S., "Numerical investigation of the effect of operating parameters on a planar solid oxide fuel cell", Energy Conversion and Management, 2015, 90:138.

[37] Lee Y. D., Ahn K. Y., Morosuk T., Tsatsaronis G., "impact assessment of a solid-oxide fuel-cell-based combined-heat-and-power-generation system", Energy, 2015, 79:455.

[38] Gao F., BlunierB., Miraoui A., Proton exchange membrane fuel cell modeling, 1st ed. Wiley-ISTE; 2012.

[39] Yan Z., Zhao P., Wang J., Dai Y., "Thermodynamic analysis of an SOFC-GT-ORC integrated power system with liquefied natural gas as heat sink", Int J Hydrogen Energy, 2013, 38(8):3352.

[40]Grondina D., Deseurea J., Ozila P., J. Chabriatb P., "Solid oxide electrolysis cell 3D simulation using artificial neural network for cathodic process description", chemical engineering research and design , 2013, 91: 134.

[41] Yang S., Chen T., Wang Y., Peng Z., Wang WG.,"Electrochemical Analysis of an Anode-Supported SOFC", Int. J. ElectrochemSci, 2013, 8: 2330.

[42] Taine J.,Iacona E., "Upscaling StatisticalMethodology for Radiative Transfer in PorousMedia New Trends", Journal of Heat Transfer Transaction of the ASME, 2012, 134: 1481.

[43] Gianfranco D., "Surface-to-Surface Radiation Exchange Effects in a 3D SOFC Stack Unit Cell", Journal Of Fuel Cell Science And Technology, 2012, 9: 1550.